

High-resolution laser spectroscopy of the hyperfine structure of high-lying levels of Nb I

Günay Başar¹, Gönül Başar², S Burçin Bayram³ and Sophie Kröger⁴

¹ Physics Engineering Department, Faculty of Science and Letters, Technical University of Istanbul, 80626 Maslak, Istanbul, Turkey

² Physics Department, Faculty of Science, Istanbul University, 34459 Vezneciler, Istanbul, Turkey

³ Department of Physics, Miami University, Oxford, OH 45056 USA

⁴ Institut für Optik und Atomare Physik, Technische Universität Berlin, Hardenbergstrasse 36, 10623 Berlin, Germany

E-mail: basar@itu.edu.tr

Received 18 February 2008

Accepted for publication 19 May 2008

Published 2 July 2008

Online at stacks.iop.org/PhysScr/78/015303

Abstract

High-resolution laser spectroscopy techniques have been applied in the wavelength range between 645 and 675 nm to measure the hyperfine structure (hfs) of high-lying levels of atomic niobium. Using Doppler-limited optogalvanic spectroscopy 20 well-resolved spectra were measured and 10 spectra using Doppler-reduced saturation absorption spectroscopy technique. We have precisely determined the magnetic dipole hfs constants A of 42 levels and electric quadrupole hfs constants B of 15 levels. For the first time 17 A constants and 5 B constants were measured.

PACS numbers: 32.10.Fn, 31.30.Gs, 32.30.Jc

1. Introduction

Precise determination of the hyperfine structure (hfs) constants has recently attracted considerable theoretical and experimental attention [1–3]. Experimental measurements of hfs constants were carried out using a variety of spectroscopic techniques involving the ground and excited levels of alkali-metal and transition-metal atoms (see, for example, [2–4]). Laser optogalvanic spectroscopy (OGS) [5] is a very sensitive and powerful detection technique for recording high-resolution spectra of atomic and molecular energy levels. Thus, OGS finds a wide range of demanding applications for studies of atomic structures, wavelength calibration, gas discharges, laboratory plasmas and excitation and ionization processes in flames.

Naturally occurring niobium (Nb) is a transition-metal and is composed of only one isotope with the odd mass number 93 and with a nuclear spin $I = 9/2$. Although the investigations of the hfs and fine structure constants of Nb have been the subject of several experimental studies [3, 6–11], parametric analysis of the data [12, 13] has shown that there is still a lack of knowledge about the

experimental hfs and fine structure constants of high-lying Nb levels. Because of the large nuclear magnetic dipole moment, $\mu_I = 6.1705(3) \mu_N$ [14] in many transitions, it is sufficient to apply Doppler-limited experimental techniques for an accurate determination of the magnetic dipole hfs constants A . The relatively small value of the electric quadrupole moment $Q = -0.36(7) \text{ b}$ [14] leads to small electric quadrupole hfs constants B and corresponding weak deviations from the interval rule. Therefore, Doppler-reduced experimental methods are needed for the precise determination of the hfs constants B . For wavelengths, intensities and classifications, we refer to the relatively old but very comprehensive list from Humphreys and Meggers [15], as well as to the wavelength tables of NBS [16] and MIT [17]. In the wavelength region between 645 and 675 nm, eight spectral lines, most with strong intensities, have already been measured [3, 11]. Using high-sensitivity Doppler-limited OGS, we investigated 20 additional lines in the same spectral region, of which 11 are listed in none of the wavelength tables [15–17]. In comparison to the OGS, the Doppler-reduced saturation absorption spectroscopy (SAS) achieves higher resolution but provides lower sensitivity. For this reason, SAS was utilized

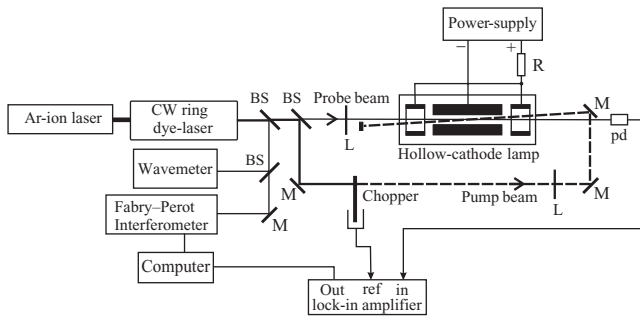


Figure 1. Schematic overview of the experimental apparatus showing the SAS measurement in the hollow-cathode lamp. BS, beam splitters; M, mirrors; R, ballast resistor; pd, photo-diode; and L, lenses.

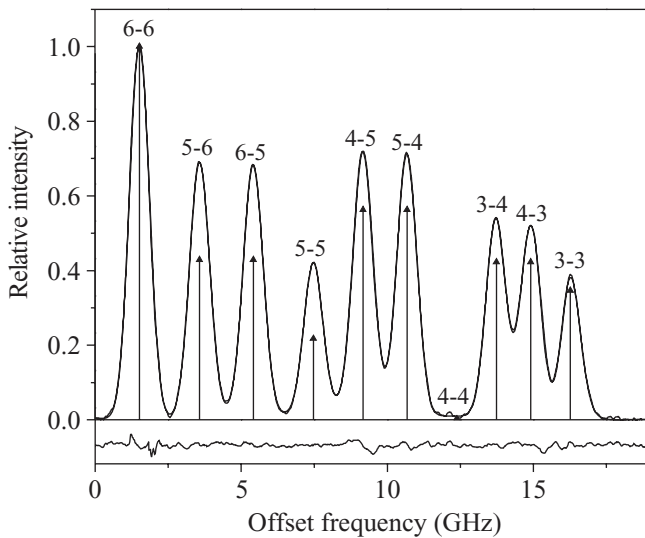


Figure 2. Intensity distribution of the OGS for the Nb I transition from 1142.79 cm^{-1} ($4d^35s^2$, $J = 3/2$) to $16\,672.00 \text{ cm}^{-1}$ ($4d^35s5p$, $J = 3/2$) at $\lambda = 643.776 \text{ nm}$. The hyperfine components are assigned by the total angular momentum F of the lower and upper hyperfine levels. The theoretical intensities are indicated by arrows relative to the intensity of the strongest hyperfine component. The spectrum is fitted using Voigt profile functions. The bottom curve shows the residuals multiplied by a factor of 3.

for 10 intense lines for additionally determining the electric quadrupole hfs constants B .

2. Experiments

An Ar-ion pumped tunable frequency-stabilized single-mode CW ring dye laser was used in the wavelength range of the dye DCM (630–675 nm). The absolute reference wavelength was determined using a wavemeter with a resolution of 0.001 nm. The relative frequency reference was given by a temperature-stabilized confocal Fabry-Perot interferometer with a free spectral range of about 300 MHz. In order to produce free Nb atoms, a liquid nitrogen-cooled, see-through, hollow-cathode lamp was used with a 15 mm long copper cathode [18] covered with a 0.125 mm Nb foil from which the Nb atoms are sputtered. The hollow-cathode lamp was operated at a current range 20–50 mA and a pressure of about 2 mbar of Ar. The excitation of Nb levels in the discharge of the hollow cathode allows the investigation of transitions starting from high-lying levels.

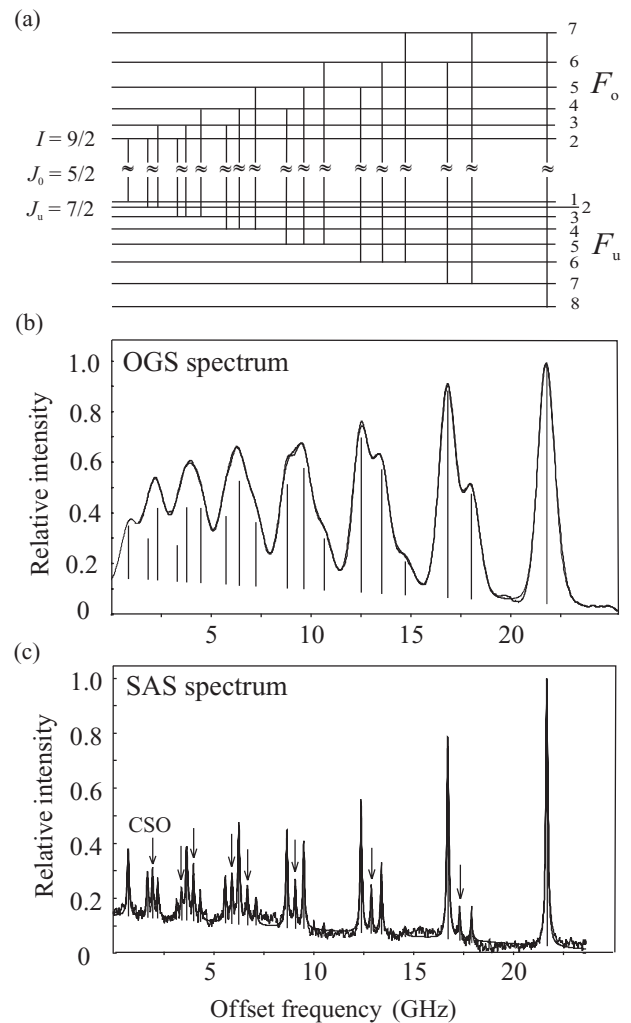


Figure 3. Nb I transition from 9497.52 cm^{-1} ($4d^45s$, $J = 7/2$) to $24\,773.03 \text{ cm}^{-1}$ ($4d^45p$, $J = 5/2$) at $\lambda = 654.461 \text{ nm}$: (a) hyperfine splitting of the upper and lower levels assigned by the total angular momentum F with the hyperfine transitions, (b) experimental intensity distribution measured by laser OGS together with the best-fitted curve, (c) experimental intensity distribution measured with SAS with COS (marked by arrows) together with the best-fitted curve.

The experimental setup for SAS measurement is schematically shown in figure 1. For SAS measurements, the laser beam is split into two beams by the beam splitter: the probe beam (a few per cent power of the main beam) and the pump beam. The two counter-propagating beams pass through the hollow-cathode lamp and they almost overlap along the lamp. With the use of two lenses, both beams were weakly focused in order to control the overlapping beam diameters and to increase the intensity of the beams in the interaction region. The pump beam was modulated by a mechanical chopper at about 3 kHz as a reference frequency to get a filtered spectrum by using a phase-sensitive lock-in amplifier. The absorption of the probe beam by the atoms belonging to the zero-velocity component along the optical axis for pump and probe beams is detected by a photodiode in the presence of a counter-propagating pump beam.

OGS measurements are performed using the typical setup similar to the setup described in [19]. The voltage change across the ballast resistor was the measured optogalvanic signal.

Table 1. Nb I transitions investigated by means of OGS, SAS or both. Intensities according to [15–17].

λ_{air} (nm)	σ (cm^{-1})	Method	Intensity			Lower-level			Upper-level		
			[15]	[16]	[17]	E (cm^{-1})	Configuration	J	E (cm^{-1})	Configuration	J
673.896	14 835.00	OGS	5	–	–	15 282.35	4d ⁴ 5s	7/2	30 117.32	4d ⁴ 5p	7/2
672.362	14 868.84	Both	150	130	2.0	8705.32	4d ⁴ 5s	3/2	23 574.14	4d ³ 5s5p	5/2
670.120	14 918.59	SAS	60	65	2.0	13 515.20	4d ³ 5s ²	7/2	28 433.74	4d ³ 5s5p	9/2
669.982 ^a	14 921.66	OGS	4h	–	–	12 692.12	4d ⁴ 5s	7/2	27 614.10	4d ³ 5s5p	5/2
668.136	14 962.89	OGS	4h	–	–	13 012.20	4d ⁴ 5s	11/2	27 974.87	4d ⁴ 5p	9/2
667.734	14 971.97	SAS	200c	150	2.3	9043.14	4d ⁴ 5s	5/2	24 015.11	4d ³ 5s5p	7/2
667.635	14 974.10	OGS	–	–	–	12 357.70	4d ⁴ 5s	9/2	27 331.80	4d ⁴ 5p	9/2
666.084	15 008.98	Both	300c	210	2.5	9497.52	4d ⁴ 5s	7/2	24 506.53	4d ³ 5s5p	9/2
663.742	15 061.92	OGS	–	–	–	12 357.70	4d ⁴ 5s	9/2	27 419.62	4d ³ 5s5p	9/2
662.722	15 085.10	OGS	–	–	–	1586.90	4d ³ 5s ²	5/2	16 672.00	4d ³ 5s5p	3/2
662.698	15 085.67	OGS	8	19	0.8	5297.92	4d ³ 5s ²	3/2	20 383.62	4d ³ 5s5p	3/2
661.668	15 109.15	OGS	6	–	0.8	4998.17	4d ³ 5s ²	1/2	20 107.36	4d ³ 5s5p	1/2
661.415	15 114.93	Both	20	35	1.4	8410.90	4d ⁴ 5s	1/2	23 525.80	4d ⁴ 5p	3/2
657.474	15 205.54	SAS	10	15	1.3	8705.32	4d ⁴ 5s	3/2	23 910.90	4d ⁴ 5p	1/2
656.725	15 222.84	OGS	–	–	–	12 136.86	4d ⁴ 5s	7/2	27 359.70	4d ⁴ 5p	5/2
656.231	15 234.31	OGS	–	–	–	11 318.09	4d ³ 5s ²	3/2	26 552.40	4d ⁴ 5p	1/2
656.027	15 239.04	OGS	–	–	–	12 357.70	4d ⁴ 5s	9/2	27 596.74	4d ⁴ 5p	7/2
655.977	15 240.20	OGS	–	–	–	9043.14	4d ⁴ 5s	5/2	24 283.34	4d ⁴ 5p	3/2
655.504	14 251.21	OGS	–	–	–	2154.11	4d ³ 5s ²	7/2	17 405.32	4d ³ 5s5p	7/2
655.163	15 259.17	OGS	8	–	0.8	16 828.52	4d ⁴ 5s	9/2	32 087.58	4d ⁴ 5p	7/2
654.461	15 275.54	Both	80c	65	1.9	9497.52	4d ⁴ 5s	7/2	24 773.03	4d ⁴ 5p	5/2
651.130	15 353.66	OGS	–	–	–	9043.14	4d ⁴ 5s	5/2	24 396.80	4d ⁴ 5p	5/2
650.496	15 368.62	OGS	–	–	–	11 344.70	4d ⁵	5/2	26 713.32	4d ⁴ 5p	3/2
650.083	15 378.41	OGS	2	–	–	12 288.25	4d ⁴ 5s	3/2	27 666.46	4d ³ 5s5p	1/2
649.785	15 385.46	SAS	1	17	1.1	4998.17	4d ³ 5s ²	1/2	20 383.62	4d ³ 5s5p	3/2
649.720	15 386.97	OGS	–	–	–	12 692.12	4d ⁴ 5s	5/2	28 079.09	4d ³ 5s5p	3/2
649.423 ^a	15 394.04	OGS	4	–	–	1586.90	4d ³ 5s ²	5/2	16 981.01	4d ³ 5s5p	5/2
643.776 ^a	15 529.07	OGS	4	–	–	1142.79	4d ³ 5s ²	3/2	16 672.00	4d ³ 5s5p	3/2
643.324	15 539.98	SAS	30	50	1.5	5297.92	4d ³ 5s ²	3/2	20 837.98	4d ³ 5s5p	5/2
643.047	15 546.67	Both	80c	85	1.9	5965.45	4d ³ 5s ²	5/2	21 512.18	4d ³ 5s5p	7/2

^aNew classification.**Table 2.** The hfs constants A and B belonging to the lower levels, which have been fixed during the fit. abmr, atomic beam magnetic resonance, lrf, laser radio-frequency double-resonance technique, lif, laser-induced fluorescence spectroscopy and OGS.

E (cm^{-1})	A (MHz)	B (MHz)	Reference	Method
1586.90	372.4853 (17)	33.341 (38)	[6]	abmr
2154.11	292.2022 (16)	44.928 (47)	[6]	abmr
11 318.09	167.3182 (25)	–5.805 (21)	[7]	lrf
11 344.70	–639.3786 (79)	–0.061 (92)	[7]	lrf
12 136.86	–502.4 (1.4)	–	[3]	lif
12 692.12	338.5 (8)	–	[3]	OGS

The high sensitivity of OGS allows one also to study lines with low-transition probabilities. Therefore, we used Doppler-limited OGS in order to measure spectral lines with low intensities. As an example, we show in figure 2 the spectrum was obtained for the excitation from the 4d³5s² level with $J = 3/2$ at 1142.79 cm^{-1} to the 4d³5s5p level with $J = 3/2$ at 16 672.00 cm^{-1} using the dye laser at the wavelength of 643.776 nm. Saturation of the strong hyperfine components appears in the spectrum, which leads to an apparent intensity enhancement of the weak hyperfine components. To demonstrate this effect, we indicated in figure 2 the theoretical hyperfine intensities by arrows relative to the intensities of the strongest hyperfine components.

We applied the high-resolution SAS technique in order to investigate some intense lines. As an example, in figure 3,

the SAS hyperfine spectrum of the transition from the 4d⁴5s level with $J = 7/2$ at 9497.52 cm^{-1} to the 4d⁴5p level with $J = 5/2$ at 24 773.03 cm^{-1} with a wavelength of 654.461 nm is compared to OGS at the same excitation wavelength. The improvement in resolution of the SAS is obvious. In contrast to the intensity increase of the weak components in the Doppler-limited OGS spectrum, the unsaturated weak components appear with intensities smaller than expected on the basis of transition probabilities in the Doppler-reduced SAS spectrum. They are sometimes hidden within the noise (see for example, the hyperfine component from $F_L = 6$ to $F_U = 7$ in figure 3). As seen in figure 3(c), crossover signals (COS) appear between weak and strong hyperfine components, which have sometimes more intensity than the weak hyperfine components and provide additional information on the line positions.

We have measured 20 transitions using Doppler-limited OGS and 10 transitions using Doppler-reduced SAS techniques. These transitions along with their corresponding wavelengths, total angular momenta, energies and intensities according to [15–17] are listed in table 1. The lines, given without an intensity entry in table 1, are newly observed lines, their wavelengths have been calculated from the energy difference of the selected known levels. Three lines, indicated in the footnote to table 1, are listed without classification in the line list reported by [15] and could be classified. For all other lines the transition classification given in [15] is confirmed.

Table 3. Magnetic dipole hfs constants A_{exp} and electric quadrupole constants B_{exp} in MHz for levels of even parity of Nb I. The wavelength given in the fourth column specifies the line which was used to determine the A and B constants; configurations and leading components (intermediate terms in successive SL -coupling) as well as A_{calc} in terms of MHz are given according to [12]. For the calculations of ΔA the mean value of our experimental A values is used. OGS, abmr, atomic beam magnetic resonance technique, lrf, laser radiofrequency double-resonance technique, lif, laser-induced fluorescence spectroscopy.

$E(\text{cm}^{-1})$	Level	λ_{air} (nm)	A_{exp}	B_{exp}	Method	Reference	A_{calc}	ΔA	
1142.79	$4d^35s^2$	$^4F_{3/2}$	643.769	643.4 (6)		OGS	This work	674	31
			566.470	634.7 (10.0)		OGS	[8]		
4998.17	$4d^35s^2$	$^4P_{1/2}$	661.665	540 (4)		abmr	[6]	570	32
			649.784	539.5 (6)		OGS	This work		
			587.776	540.1 (0.9)		SAS	This work		
			587.776	537.4 (6.0)		lrf	[7]		
5297.92	$4d^35s^2$	$^4P_{3/2}$	643.320	497.1 (6)	59 (5)	OGS	[10]	447	-50
			598.322	497.7569 (16)	59.902 (14)	SAS	This work		
			598.322	495.5 (6.0)	30 (35)	lrf	[7]		
5965.45	$4d^35s^2$	$^4P_{5/2}$	643.044	343.2 (5)	-93 (15)	OGS	[10]	435	92
			586.643	343.1670 (5)	-80.454 (9)	SAS	This work		
			586.643	341.3 (10.0)	-122.3 (30.0)	lrf	[7]		
			643.046	343.4 (1.1)	-76 (5)	OGS	[8]		
8410.90	$4d^45s$	$^5D^4D_{1/2}$	661.415	1996 (1)		OGS	[12]	2022	26
			570.647	1997.0 (1.1)		SAS	This work		
			570.647	2001.7 (10.0)		lrf	[7]		
			661.415	2003 (11)		OGS	[8]		
8705.32	$4d^45s$	$^5D^4D_{3/2}$	657.471	-143.4 (3)	-9 (3)	OGS	[12]	-126	18
			672.362	-143.6 (5)	-12 (4)	SAS	This work		
			580.401	-143.3225 (217)	-10.761 (178)	lrf	[7]		
			576.032	-136.9 (6.0)	-69 (35)	SAS	This work		
			672.362	-142.7 (1.6)	7 (17)	OGS	[10]		
9043.14	$4d^45s$	$^5D^4D_{5/2}$	667.733	-408.0 (4)	32 (5)	OGS	[12]	-394	-14
			587.467	-407.8606 (43)	35.060 (75)	SAS	This work		
			583.860	-408.6 (10.0)	38.9 (30.0)	lrf	[7]		
9497.52	$4d^45s$	$^5D^4D_{7/2}$	654.461	-477.0 (5)	116 (12)	OGS	[8]	-496	19
			666.084	-477.0 (5)	120 (22)	SAS	This work		
			591.943	-477.0373 (35)	126.899 (81)	lrf	[7]		
			590.057	-474.4 (2.0)	90 (35)	OGS	[10]		
			654.461	-477.3 (1.8)	88 (50)	OGS	[12]		
			670.988	-478.0 (1.7)	98 (30)	OGS	[12]		
			832.093	-476.9 (6)	131 (8)	lrf	[12]		
			666.084	-475 (2)	86 (50)	OGS	[12]		
12 288.25	$4d^45s$	$^3F^4F_{3/2}$	650.090	-592 (2)		OGS	This work	-599	7
			912.507	-590 (30)		OGS	[12]		
12 357.70	$4d^45s$	$^3F^4F_{9/2}$	663.742	740 (2)		OGS	This work	597	-145
			656.027	744 (3)		OGS	This work		
13 012.20	$4d^45s$	$^3G^4G_{11/2}$	668.145	699 (5)		OGS	This work	672	-27
13 515.20	$4d^45s$	$^3F^2F_{7/2}$	670.120	137.6 (5)	-25 (12)	SAS	This work	222	85
			581.190	136.9050 (6)	-48.916 (14)	lrf	[7]		
15 282.35	$4d^45s$	$^3D^4D_{7/2}$	673.896	988 (5)		OGS	This work	882	-106
				957.3 (5.0)		OGS	[10]		
16 828.52	$4d^45s$	$^1G^2G_{9/2}$	655.163	743.6 (1.2)		OGS	This work	754	10

To take into account the saturation broadening, the optogalvanic spectra were fitted using Voigt profile functions for the determination of the magnetic dipole hfs constants A of the energy levels. The influence of the electric quadrupole hfs constants B was neglected during the fit to the Doppler-limited optogalvanic spectra. All the spectra with well-separated hyperfine components are fitted with individual profile and intensity parameters for each hyperfine component (see, for example, figure 2). To analyze the spectra of lines with partially unresolved hfs, the profile and the intensity parameters of unresolved components were coupled to other components with the same total angular momentum difference ΔF between upper and lower levels. In some cases the hfs constant A of the lower level was fixed if the values

were already known from atomic beam magnetic resonance measurements [6], laser radio-frequency double-resonance measurements [7], laser-induced fluorescence spectroscopy or laser OGS measurements [3]. A list of the hfs constants A and B used and the corresponding energy levels are given in table 2.

For the analysis of the SAS spectra, the experimental intensity distribution is fitted to a sum function of Lorentzian and Gaussian profiles taking into account the COS. The same profile parameters are used for all hyperfine components, but individual intensity parameters are used for each component. For these Doppler-reduced spectra, both hfs constants A and B are taken into account and fitted as free parameters.

Table 4. Magnetic dipole hfs constants A_{exp} and electric quadrupole constants B_{exp} in terms of MHz for levels of odd parity of Nb I. The wavelength given in the fourth column specifies the line, which was used to determine the A and B constants; configurations and leading components (intermediate terms in successive SL -coupling) as well as A_{calc} are given according to [13]. OGS, lrf, laser radiofrequency double-resonance technique, lif, laser-induced fluorescence spectroscopy. For the calculations of ΔA the mean value of our experimental A values is used.

$E(\text{cm}^{-1})$	Level	$\lambda_{\text{air}}(\text{nm})$	A_{exp}	B_{exp}	Method	Reference	A_{calc}	ΔA	
16 672.00	4d ³ 5s5p	$^4F^5F^6G_{3/2}$	662.722	-340.6 (8) ^a		OGS	This work	-322	-18
			643.769	-339.1 (1.0)		OGS	This work		
			471.579	-339.1 (1.0)		lif	[3]		
16 981.01	4d ³ 5s5p	$^4F^5F^6G_{5/2}$	649.419	382 (1)		OGS	This work	367	-15
			475.141	386 (10)		lif	[3]		
17 405.32	4d ³ 5s5p	$^4F^5F^6G_{7/2}$	655.504	601.4 (7) ^a		OGS	This work	583	-18
			470.830	601 (3)		lif	[3]		
			478.994	601 (4)		lif	[3]		
20 107.36	4d ³ 5s5p	$^4F^5F^4D_{1/2}$	661.665	792 (3)		OGS	This work	-339	-1131
20 383.62	4d ³ 5s5p	$^4F^5F^4D_{3/2}$	662.696	598 (3) ^a		OGS	This work	668	70
			649.784	597.8 (5)	-13 (4)	SAS	This work		
20 837.98	4d ³ 5s5p	$^4F^5F^4D_{5/2}$	643.320	808.8 (4)	-14 (6)	SAS	This work	822	74
			672.19	803 (6)		OGS	[3]		
21 512.18	4d ³ 5s5p	$^4F^5F^4D_{7/2}$	643.044	872.8 (5)	-27 (6)	SAS	This work	867	-6
			832.093	872.0 (7)		lif	[12]		
			643.044	873.2 (5)		OGS	[12]		
23 525.80	4d ³ 5s5p	$^4F^3F^2D_{3/2}$	661.415	593.8 (4)	-13 (3)	SAS	This work	556	-37
			611.415	595 (7)		OGS	[3]		
23 574.14	4d ³ 5s5p	$^4F^5F^4F_{5/2}$	672.362	514.1 (2)	67 (5)	SAS	This work	496	-18
			672.362	514.5 (9)	94 (30)	OGS	[12]		
			918.695	515.7 (8)	-	OGS	[3]		
23 910.90	4d ³ 5s5p	$^2P^3P^2S_{1/2}$	657.471	627.4 (6)	-	SAS	This work	498	-129
24 015.11	4d ³ 5s5p	$^4F^5F^4F_{7/2}$	667.733	591.8 (3)	108 (17)	SAS	This work	579	-13
			919.762	595 (5)	-	OGS	[3]		
24 283.34	4d ⁴ 5p	$^5D^6P_{3/2}$	655.977	93 (1) ^a		OGS	This work	492	399
24 396.80	4d ⁴ 5p	$^5D^6F_{5/2}$	651.130	227.6 (6) ^a		OGS	This work	206	-22
			670.988	227 (3) ^b		OGS	[12]		
24 506.53	4d ³ 5s5p	$^4F^5F^4F_{9/2}$	666.084	593.0 (4)	148 (37)	SAS	This work	622	29
			666.084	594 (3)	70 (50)	OGS	[12]		
24 773.03	4d ³ 5s5p	$^4F^3F^2D_{5/2}$	654.461	170.1 (5)	-11 (7)	SAS	This work	321	151
			654.461	170.2 (1.9)	-24 (30)	OGS	[12]		
26 552.40	4d ⁴ 5p	$^5D^6D_{1/2}$	656.231	428.8 (1.6) ^a		OGS	This work	430	1
			584.178	430.1 (5)		lrf	[7]		
26 713.32	4d ⁴ 5p	$^5D^6D_{3/2}$	650.496	107.1 (1.5) ^a		OGS	This work	299	192
			606.782	108.6 (4)	-19.6 (3.0)	lrf	[7]		
27 331.80	4d ³ 5s5p	$^2G^3G^4H_{9/2}$	667.635	392.6 (7) ^a		OGS	This work	463	71
27 359.70	4d ⁴ 5p	$^5D^4D_{5/2}$	656.725	-25.5 (2.0) ^a		OGS	This work	219	244
27 419.62	4d ³ 5s5p	$^4P^5P^6D_{9/2}$	663.742	405 (2)		OGS	This work	492	87
			855.850	405.4 (9)	-94 (20)	lif	[12]		
27 596.74	4d ⁴ 5p	$^5D^4D_{7/2}$	656.027	-149 (2)		OGS	This work	115	264
27 614.10	4d ³ 5s5p	$^2P^3P^4P_{5/2}$	669.967	615 (2) ^a		OGS	This work	621	6
27 666.46	4d ³ 5s5p	$^2P^3P^4D_{1/2}$	650.090	726 (4)		OGS	This work	603	-47
27 974.87	4d ³ 5s5p	$^4P^5P^6D_{9/2}$	668.145	504 (5)		OGS	This work	465	-39
28 079.09	4d ³ 5s5p	$^4P^5P^4P_{3/2}$	649.720	678 (6) ^a		OGS	This work	237	-441
28 433.74	4d ³ 5s5p	$^4F^3F^2G_{9/2}$	670.120	179.5 (4)	-48 (12)	SAS	This work	312	133
30 117.32	4d ³ 5s5p	$^2G^3G^4F_{9/2}$	673.896	622 (5)		OGS	This work	587	-35
32 087.58	4d ⁴ 5p	$^3H^2G_{7/2}$	655.163	316 (2)		OGS	This work	399	83

^aA constant of the lower level fixed during the fit according to table 2.

^bTyping error in [12].

3. Results

The magnetic dipole hfs constants A of 14 energy levels of even parity and those of 28 energy levels of odd parity have been determined experimentally. Of the total 42 measured magnetic dipole hfs constants A , 17 were measured for the first time. The electric quadrupole hfs constants B were obtained only for transitions measured using SAS technique. The hfs constants B of the 6 levels of even parity and those of 9 levels of odd parity were determined; 6 are given for the first time. All of the measured hfs constants A and B are compiled in table 3 for the even parity and in table 4 for the odd parity, together with the specification of the wavelengths and the methods used to determine them. The hyperfine spectrum of each of the investigated lines has been recorded and fitted 10 times. The given hfs A and B values are the mean of the best values of the ten fits and the error margins are the standard deviations. The cases where the hfs constants of the lower level were fixed during the fit are indicated in the footnote to table 4.

If for a level the hfs A and B values were not measured for the first time, previous values from literature are also listed in tables 3 and 4. The experimental hfs constants A and B compared to the different sources agree within the limit of error with our results. The hfs constants A and B of the level $4d^4 5s^4 D_{3/2}$ at 8705.32 cm^{-1} are out of the error margin compared to [10], but our values agree with the values listed in [7, 11]. Additionally, in tables 3 and 4 the calculated hfs constants A_{calc} , which result from a parametric analysis of the hfs done in [12, 13] and the difference between experimental and calculated values ΔA is given.

For the three levels of even parity, $12\,357.70 \text{ cm}^{-1}$ ($J = 9/2$), $13\,012.20 \text{ cm}^{-1}$ ($J = 11/2$) and $16\,828.52 \text{ cm}^{-1}$ ($J = 9/2$), hfs A values are reported in the present paper for the first time. For the latter two levels, our experimental values agree well with the theoretical predictions. Only the level $12\,357.70 \text{ cm}^{-1}$ shows a stronger deviation. In the fine structure calculation [12], for this level the experimental g -factor also deviates from the calculated one. The energetically close-lying level with same J value, $12\,102.12 \text{ cm}^{-1}$ shows a deviation between experimental and calculated hfs A values of about 100 MHz with the opposite sign [12]. Both these facts point out an inaccurate calculation of the mixing of the eigenfunctions of the $12\,357.70$ and $12\,102.12 \text{ cm}^{-1}$ energy levels.

For the levels of odd parity, 13 new hfs A values are presented. Five of them show a deviation higher than 200 MHz between experimental values and theoretical predictions [13], indicating inaccuracies in the fine structure wavefunctions. This especially concerns levels with small J values. The energy level $20\,107.36 \text{ cm}^{-1}$ ($J = 1/2$, $A_{\text{exp}} = 792(3) \text{ MHz}$) with $\Delta A > 1000 \text{ MHz}$ has the strongest deviation. For this level, the difference between experimental and calculated g -factor in the fine structure calculation [13] is also large. For the neighboring level with same J value at $19\,623.96 \text{ cm}^{-1}$, no experimental hfs A value is known. The predicted value for this level lies with $A_{\text{calc}} = 1509 \text{ MHz}$ [13] close to the hfs A_{exp} of the level at $20\,107.36 \text{ cm}^{-1}$. The mixing of these two levels seems to be not well reproduced by the fine structure

calculations [13]. Therefore, a deviation of the experimental hfs A from the calculated one is also expected for the $19\,623.96 \text{ cm}^{-1}$ level.

4. Conclusions

We present new experimental data on high-lying levels in Nb using the SAS technique to measure the magnetic dipole and the electric quadrupole hfs constants A and B , respectively. Additionally, we used the OGS technique in order to determine the magnetic dipole hfs constants A . With the present work, the experimental hyperfine data for the levels of atomic Nb are extended. In a comparison with the calculated hfs A values, our experimental results show a good agreement for the levels of even parity. For the levels of odd parity, the deviations are higher, which indicate the higher uncertainties of the wavefunctions for the odd configurations. This fact confirms the importance of expanding the manifold of the experimental data.

Acknowledgments

GB acknowledges the Istanbul University for its support under project no. UDP-932/18042007 and SBB acknowledges the Research Corporation for its support under grant no. CC7133.

References

- [1] Safronova U I, Cowan T E and Safronova M S 2006 *J. Phys. B: At. Mol. Opt. Phys.* **39** 749
- [2] Auzinsh M, Bluss K, Ferber R, Gahbauer F, Jarmola A, Safronova M S, Safronova U I and Tamanis M 2007 *Phys. Rev. A* **75** 022502
- [3] Kröger S 2007 *Eur. Phys. J. D* **41** 55
- [4] Yei W, Sieradzian A, Cerasuolo E and Havey M D 1998 *Phys. Rev. A* **57** 3419
- [5] Barbieri B, Beverini N and Sasso A 1990 *Rev. Mod. Phys.* **62** 603
- [6] Büttgenbach S, Dicke R, Gebauer H, Herschel M and Meisel G 1975 *Z. Phys. A* **275** 193
- [7] Frankel L, Bengtsson C, Hanstrop D, Nyberg A and Persson J 1988 *Z. Phys. D* **8** 171
- [8] Singh R and Rao G N 1989 *Phys. Scr.* **40** 170
- [9] Lauranto H M, Auterinen I H, Kajava T T, Nyholm K M and Salomaa R R E 1990 *Appl. Phys. B* **50** 323
- [10] Singh R, Thareja R K and Rao G N 1992 *J. Opt. Soc. Am. B* **9** 493
- [11] Bouzed A, Kröger S, Zimmermann D, Kronfeldt H-D and Guthöhrlein G 2003 *Eur. Phys. J. D* **23** 57
- [12] Kröger S and Bouzed A 2003 *Eur. Phys. J. D* **23** 63
- [13] Kröger S, Öztürk I K, Acar F G, Başar Gü, Başar Gö and Wyart J-F 2007 *Eur. Phys. J. D* **41** 61
- [14] Lederer C M and Shirley V S 1978 *Tables of Isotopes* 7th edn (New York: Wiley)
- [15] Humphreys C I and Meggers W F 1945 *J. Res. Natl Bur. Stand.* **34** 478
- [16] Meggers W F, Corliss C H and Scribner B F 1975 *Tables of Spectral Line Intensities. Part I. Arranged by Elements* 2nd edn (Washington, DC: National Bureau of Standards)
- [17] Phelps F M 1991 *Wavelength Tables Volume 2: Wavelength by Element* (Cambridge, MA: MIT Press)
- [18] Messnarz D and Guthöhrlein G H 2000 *Eur. Phys. J. D* **12** 269
- [19] Kronfeldt H D and Başar G 1995 *Phys. Scr.* **51** 227